

The Signature of Patchy Reionization in the Polarization Anisotropy of the CMB

Olivier Doré⁽¹⁾, Gil Holder⁽²⁾, Marcelo Alvarez⁽³⁾, Ilian T. Iliev⁽¹⁾, Garrelt Mellema⁽⁴⁾, Ue-Li Pen⁽¹⁾, Paul R. Shapiro⁽⁵⁾

(1) *Canadian Institute for Theoretical Astrophysics, University of Toronto,
60 St. George Street, Toronto, ON M5S 3H8, Canada*

(2) *Department of Physics, McGill University, Montreal, QC H3A 2T8, Canada*

(3) *Kavli Institute for Particle Astrophysics and Cosmology,
Stanford University, P.O. Box 20450, MS 29, Stanford, CA, 94309, USA*

(4) *Stockholm Observatory, AlbaNova University Center,
Stockholm University, SE-106 91 Stockholm, Sweden*

(5) *Department of Astronomy, University of Texas, Austin, 78712-1083, USA*

(Dated: November 5, 2018)

The inhomogeneous ionization state of the universe when the first sources of ionizing radiation appeared should lead to anisotropies in the polarization of the cosmic microwave background. We use cosmological simulations of the process by which the first sources ionized the intergalactic medium to study the induced polarization anisotropies. We find that the polarization anisotropies have rms of order $\sim 0.01 \mu K$, and local peak values of $\sim 0.1 \mu K$, smaller than those due to gravitational lensing on small scales. The polarization direction is highly coherent over degree scales. This directional coherence is not expected from either primary anisotropy or gravitational lensing effects, making the largest signals due to inhomogeneous ionization relatively easy to isolate, should experiments achieve the necessary very low noise levels.

I. INTRODUCTION

The cosmic microwave background (CMB) has greatly enhanced our understanding of cosmology in the last decade through precise measurements of the conditions of the universe at $z \sim 1100$. As new CMB polarization experiments target higher resolution and better sensitivity astrophysical processes at intermediate redshifts ($z \lesssim 30$) will become increasingly important as they leave their faint imprints and distortions in the CMB.

This task seems well underway on the large scales, where linear perturbation is valid. The unambiguous signature of reionization on those scales has been well measured as an excess of powers in the so-called E modes generated by scalar and tensor perturbations to the background metric (Page et al. [1]). But experiments currently being built or designed aim at detecting the fainter B modes, generated only by tensor perturbation to the metric. However, at smaller angular scales, the picture is more complicated and less certain. All types of perturbations beyond linear order produce both E and B modes and gravitational lensing, for example, will transfer power from E to B modes. Furthermore, at smaller scales, the details of the reionization history will matters critically. As such, controlling exactly the extent to which those non-linear term contribute to the CMB polarization signal is an important task we adress in this paper, focusing on the signature of reionization at small angular scales.

One possible source of polarization anisotropy at small scales is indeed Thomson scattering by free electrons at the time when the universe goes through a transition from neutral to ionized at some time $z > 6$. The inhomogeneous distribution of ionized and neutral patches might be expected to provide an enhanced level of inhomogeneity in the Thomson optical depth; through Thomson scattering of the quadrupole component of the anisotropy of the CMB it could be possible to get significant CMB polarization anisotropy on small scales. Estimates of this signal using semi-analytic techniques (Weller [2], Hu [3], Liu et al. [4]) suggested that this signal is likely to be subdominant. Recent estimates Mortonson and Hu [5] largely agree with this prognosis, but there is certain disagreement between simulations and analytic models of other reionization observables like redshifted 21-cm line of hydrogen and CMB temperature anisotropies from kinetic Sunyaev-Zel'dovich effect (Mellema et al. [6], Iliev et al. [7, 8]). For example, recent simulations (Iliev et al. [7, 8]) found a surprisingly high contribution to the expected level of momentum transfer to CMB photons due to bulk motions in the partially polarized epoch of reionization, suggesting that the bubble size distributions assumed in the analytical reionization models are unrealistic and that perhaps scattering effects in general may have been underestimated.

A large source of complication for understanding CMB polarization measurements will be gravitational lensing of the primary CMB polarization pattern. To first order, gravitational lensing does not rotate the plane of polarization but does distort the CMB anisotropy spatial pattern and induce higher order correlations in an intrinsically Gaussian distribution. These higher order correlations can be used to estimate the level of distortion caused by gravitational lensing and thus remove the induced distortions that could otherwise mimic the imprint of gravitational radiation generated during an initial period of cosmic inflation (Knox and Song [9], Seljak and Hirata [10]). Patchy reionization could provide a significant source of noise for this cleaning process and could lead to a fundamental floor to the

accuracy to which we could measure gravitational radiation signatures in the CMB.

In this work we use recent simulations of reionization that include self-consistent radiative transfer during the entire reionization process coupled with a accurate treatment of the coherence of the primordial quadrupole anisotropy to calculate the expected polarization anisotropy of the CMB due to the reionization of the universe.

In the next section we describe our simulations, followed by a description of the numerical techniques for generating polarization maps from the simulation outputs. We then discuss the levels of polarization that we find and compare with analytic estimates. We follow this with a discussion of implications for cleaning of gravitational lensing effects and close with a summary and discussion of future directions.

II. SIMULATIONS

Our simulations follow the evolution of a comoving simulation volume of $(100 h^{-1} \text{Mpc})^3$. Our basic methodology and simulation parameters were described in detail in Iliev et al. [11], Mellema et al. [12] and Iliev et al. [13]. Here we provide just a brief summary. First we perform a very large pure dark matter simulations of early structure formation, with $1624^3 \approx 4.3$ billion particles and 3248^3 grid cells [37] using the particle-mesh code PMFAST (Merz et al. [14]). Such a high mass resolution allows for reliable identification (with 100 particles or more per halo) of all collapsed dark matter halos with masses $\sim 2 \times 10^9 M_\odot$ or larger. We save the detailed halo catalogs, which contain the halo positions, masses and properties, in up to 100 time slices starting from high redshift ($z \sim 30$) down to the observed end of reionization at $z \sim 6$ or later. We also save the corresponding density and bulk peculiar velocity fields at the resolution of the radiative transfer grid. Since radiative transfer simulations at the full grid size of our N-body simulations are not practical, we follow the radiative transfer on coarser grids, of sizes $203^3 = (3248/16)^3$ or 406^3 .

For this study we assume two flat Λ CDM cosmologies, the first with parameters $(\Omega_m, \Omega_\Lambda, \Omega_b, h, \sigma_8, n) = (0.27, 0.73, 0.044, 0.7, 0.9, 1)$ [15, hereafter WMAP1], and $(\Omega_m, \Omega_\Lambda, \Omega_b, h, \sigma_8, n) = (0.24, 0.76, 0.042, 0.73, 0.74, 0.95)$ [16, hereafter WMAP3], where Ω_m , Ω_Λ , and Ω_b are the total matter, vacuum, and baryonic densities in units of the critical density, h is the Hubble constant in units of $100 \text{ km s}^{-1} \text{Mpc}^{-1}$, σ_8 is the standard deviation of linear density fluctuations at present on the scale of $8 h^{-1} \text{Mpc}$, and n is the index of the primordial power spectrum. We use the CMBfast transfer function (Seljak and Zaldarriaga [17]).

All identified halos are assumed to be sources of ionizing radiation and each is assigned a photon emissivity proportional to its total mass, M , according to

$$\dot{N}_\gamma = f_\gamma \frac{M \Omega_b}{\mu m_p t_s \Omega_0}, \quad (1)$$

where t_s is the source lifetime, m_p is the proton mass, μ is the mean molecular weight and f_γ is an assumed photon production efficiency which depends on the number of photons produced per stellar atom, the star formation efficiency (i.e. what fraction of the baryons are converted into stars) and the escape fraction (i.e. how many of the produced ionizing photons escape the halos and are available to ionize the IGM).

The radiative transfer is followed using our fast and accurate ray-tracing photoionization and non-equilibrium chemistry code C²-Ray (Mellema et al. [18]). The code has been tested in detail for correctness and accuracy against available analytical solutions and a number of other cosmological radiative transfer codes (Mellema et al. [18], Iliev et al. [19]). The radiation is traced from every source on the grid to every cell using short-characteristic ray-tracing.

We have performed four radiative transfer simulations with WMAP1 background cosmology and two simulations with WMAP3 parameters. Each of these sets share the source lists and density fields given by the underlying N-body simulation, but adopt different assumptions about the source efficiencies and the sub-grid density fluctuations. The WMAP1 and WMAP3 simulations use different random seeds. The runs and notation are the same as in Mellema et al. [12] and Iliev et al. [13]. Simulations f2000 and f250 assume $f_\gamma = 2000$ and 250, respectively, and no sub-grid gas clumping, while f2000C and f250C adopt the same respective efficiencies, $f_\gamma = 2000$ and 250, but also add a sub-grid gas clumping, $C(z) = \langle n^2 \rangle / \langle n \rangle^2$, which evolves with redshift according to

$$C_{\text{subgrid}}(z) = 27.466 e^{-0.114z + 0.001328 z^2}. \quad (2)$$

in WMAP1 cosmology and as

$$C_{\text{sub-grid}}(z) = 26.2917 e^{-0.1822z + 0.003505 z^2}. \quad (3)$$

for WMAP3 cosmology. These fits were obtained from another two high-resolution PMFAST N-body simulation, with box sizes $(3.5 h^{-1} \text{Mpc})^3$ and a computational mesh and number of particles of 3248^3 and 1624^3 , respectively. These parameters correspond to a particle mass of $10^3 M_\odot$ and minimum resolved halo mass of $10^5 M_\odot$. This box

size was chosen so as to resolve the scales most relevant to the gas clumping - on scales smaller than these the gas fluctuations would be below the Jeans scale, while on larger scales the density fluctuations are already present in our computational density fields and should not be doubly-counted. The expression in equation (2) excludes the matter inside collapsed minihalos (halos which are too small to cool atomically, and thus have inefficient star formation) since these are shielded, unlike the generally optically-thin IGM. This self-shielding results in a lower contribution of the minihalos to the total number of recombinations than one would infer from a simple gas clumping argument ([20, 21, 22]). The effect of minihalos could be included as sub-grid physics as well, see (Ciardi et al. [23], McQuinn et al. [24]). This results in slower propagation of the ionization fronts and further delay of the final overlap. The halos that can cool atomically are assumed here to be ionizing sources and their recombinations are thus implicitly included in the photon production efficiency f_γ through the corresponding escape fraction. Such treatment would tend to overestimate the effects from small-scale clumping (except for the minihalo effects) since we assume that the gas follows the dark matter distribution at small scales and we ignore the gradual smoothing of the gas density field due to pressure effects in the ionized regions. Thus, the cases with and without sub-grid clumping should be considering as bracketing the effect of gas clumping from above and below.

III. PROPAGATING LINEARLY POLARIZED CMB PHOTON PLANES IN THE SIMULATION

Linear polarization of the CMB is generated by the Thomson scattering of incoming radiation with a quadrupole anisotropy radiation pattern (see for example the general formalism for CMB polarization described by Zaldarriaga and Seljak [25]). In principle we can distinguish three different origins for the quadrupole anisotropies: primordial from projection of the Sachs-Wolfe temperature, intrinsic quadrupole from scattering (projection of the Doppler effect) and kinematic quadrupole from second-order Doppler effects. We will, however, neglect the latter two following the results and arguments from Hu [3].

As we will show below, the quadrupole anisotropy in the radiation is spatially slowly varying, so the dominant source of small scale fluctuations in the polarization are from fluctuations in the number of electrons that are the targets for Thomson scattering. We use the simulations to provide the free electron distribution; to calculate the polarization anisotropy we must calculate the quadrupole for each z and its correlation properties over large scales. Past work investigating polarization anisotropies due to late time Thomson scattering has often assumed a constant quadrupole; a notable exception is the work of Amblard and White [26], where they used a very low resolution realization of the universe to keep track of CMB anisotropy at different locations. We instead use analytic tools to keep track of the covariance between observed quadrupoles at different locations and epochs in the universe.

A. Quadrupole as a function of time and Q,U maps generation

We closely follow Hu [3] and Portsmouth [27] in our formalism. The polarization generated at a position \mathbf{x} ($\hat{\mathbf{x}}$ the associated unit vector), with the observer being at the origin of the reference frame, and τ being the conformal lookback time ($\tau = 0$ today and $\|\mathbf{x}\| = \tau$) can be written as

$$[Q \pm iU](\hat{\mathbf{n}}) = \frac{1}{10} \sqrt{\frac{3}{4\pi}} \int_0^\tau d\chi g \sum_{m=-2}^2 a_{2m}(\mathbf{x}, \chi)_{\pm 2} Y_2^m(\hat{\mathbf{n}}) \quad (4)$$

$$g(\mathbf{x}, \chi) = \dot{\tau}_T(\chi) e^{-\tau_T(\chi)} \quad (5)$$

where $_{\pm 2}Y_{2m}$ are defined as *e.g.* in Hu and White [28]. The optical depth to Thomson scattering τ_T is given by

$$\tau_T(\tau) = \sigma_T \int_0^\tau n_e(\chi) d\chi \quad (6)$$

and the quadrupole at any point is

$$a_{2m}(\mathbf{x}) = -4\pi \int d^3\mathbf{k} e^{i\mathbf{k}\cdot\mathbf{x}} \Delta_2(\mathbf{k}, \tau) Y_{2m}^*(\hat{\mathbf{k}}) \quad (7)$$

$$\Delta_\ell(\mathbf{k}, \tau) = \Delta_\ell(k, \tau) \Phi_i(\mathbf{k}) \quad (8)$$

$$\Delta_\ell(k, \tau) = \frac{3}{10} j_\ell[k(\tau - \tau_{rec})] + \frac{9}{5} \int_0^{\tau - \tau_{rec}} d\chi' j_\ell(k\chi') \frac{\partial}{\partial \tau} \left(\frac{D}{a} \right) (\tau - \chi') \quad (9)$$

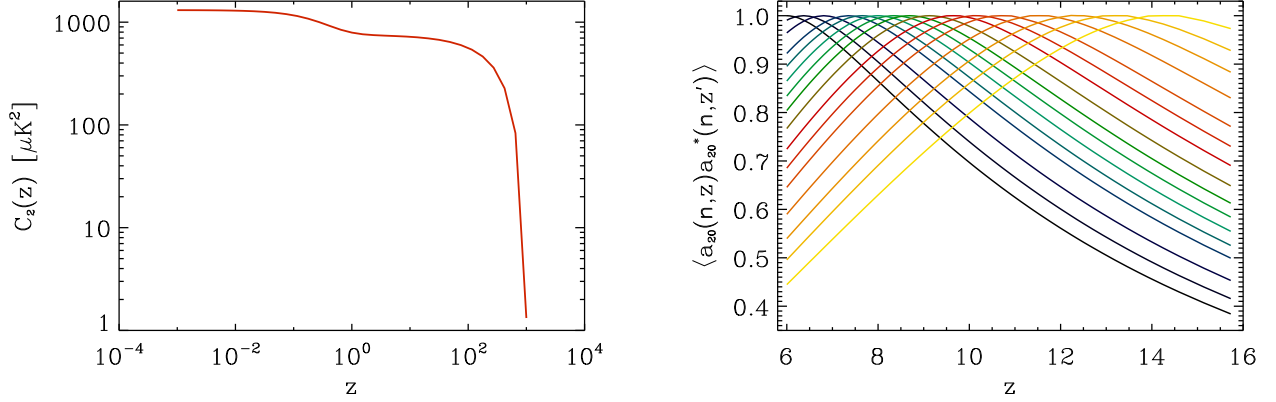


FIG. 1: *Left panel:* Quadrupole C_2 as a function of z . *Right panel:* Correlation $\langle a_{2m}(0,0,\tau(z))a_{2m'}^*(0,0,\tau(z')) \rangle$ for $(m,m') = (2,2)$ where z and z' correspond to the center of each box. Each line/color corresponds to a given z' . The correlation peaks to 1 of course when $z = z'$. Similar results are obtained for $(m,m') = (1,1)$ or $(0,0)$.

where Φ_i is the initial gravitational potential and $\Delta_\ell(k, \tau)$ is the transfer function. Computing a_{2m} at all cells of the simulation volume is computationally prohibitive but fortunately not necessary since the quadrupole is hardly varying within a 100 h/Mpc box as we show below by computing the auto-correlation of $a_{2m}(\mathbf{x})$. It is varying from box to box as new modes enter the horizon but only slowly, since the kernel convolving the gravitational potential $\Phi_i(\mathbf{k})$ in Eq. 7 is broad.

To illustrate this let us compute the covariances $\langle a_{2m}(\mathbf{x})a_{2m'}^*(\mathbf{x}') \rangle$ where $\langle \rangle$ denotes ensemble average. Following Portsmouth [27] we obtain for $\mathbf{x} \neq \mathbf{x}'$

$$\langle a_{2m}(\mathbf{x})a_{2m'}^*(\mathbf{x}') \rangle = 5(4\pi)^{5/2}(-1)^m \sum_{\ell=0}^2 (-1)^\ell \begin{pmatrix} 2 & 2 & 2\ell \\ 0 & 0 & 0 \end{pmatrix} \begin{pmatrix} 2 & 2 & 2\ell \\ -m & m' & m'-m \end{pmatrix} K_{2\ell}(\mathbf{x} - \mathbf{x}', \tau, \tau') Y_{2\ell, m'-m}^*(\hat{\mathbf{x}} - \hat{\mathbf{x}}') \quad (10)$$

with

$$K_\ell(\mathbf{x}, \tau, \tau') = \int k^2 dk \Delta_2(k, \tau) \Delta_2(k, \tau') \mathcal{P}_{\Phi\Phi}^0(k) j_\ell(k|\mathbf{x}|) \quad (11)$$

and where

$$\langle \Phi_i(\mathbf{k}) \Phi_i^*(\mathbf{k}') \rangle = \delta_D(\mathbf{k} - \mathbf{k}') \mathcal{P}_{\Phi\Phi}^0(k) . \quad (12)$$

whereas we obtain for $\mathbf{x} = \mathbf{x}'$,

$$\langle a_{2m}(\mathbf{x})a_{2m'}^*(\mathbf{x}') \rangle = \delta_{mm'} C_2(\tau) \quad (13)$$

with

$$C_2(\tau) = (4\pi)^2 \int k^2 dk \Delta_2^2(k, \tau) \mathcal{P}_{\Phi\Phi}^0(k) . \quad (14)$$

The important results of this section are summarized in Fig.1 where we see in the left panel the evolution of the quadrupole C_2 as a function of redshift, and in the right panel the correlation between $a_{22}(z)$ and $a_{22}(z')$ as seen by observers at various redshifts along our line of sight. The redshifts were chosen to match the center of the simulation boxes. We see from this plot that two consecutive boxes would have a a_{22} 's correlated at more than 99%. However this correlation drops to 50% for the most distant boxes. This suggests that the polarized signal from patches of ionization at the beginning of reionization could be significantly misaligned with that generated at the end of reionization, provided reionization happens relatively slowly. Conversely, if the universe makes a transition from mainly neutral to mainly ionized over a small redshift range then the polarization anisotropy will be sourced by a quadrupole that is effectively constant in both direction and amplitude.

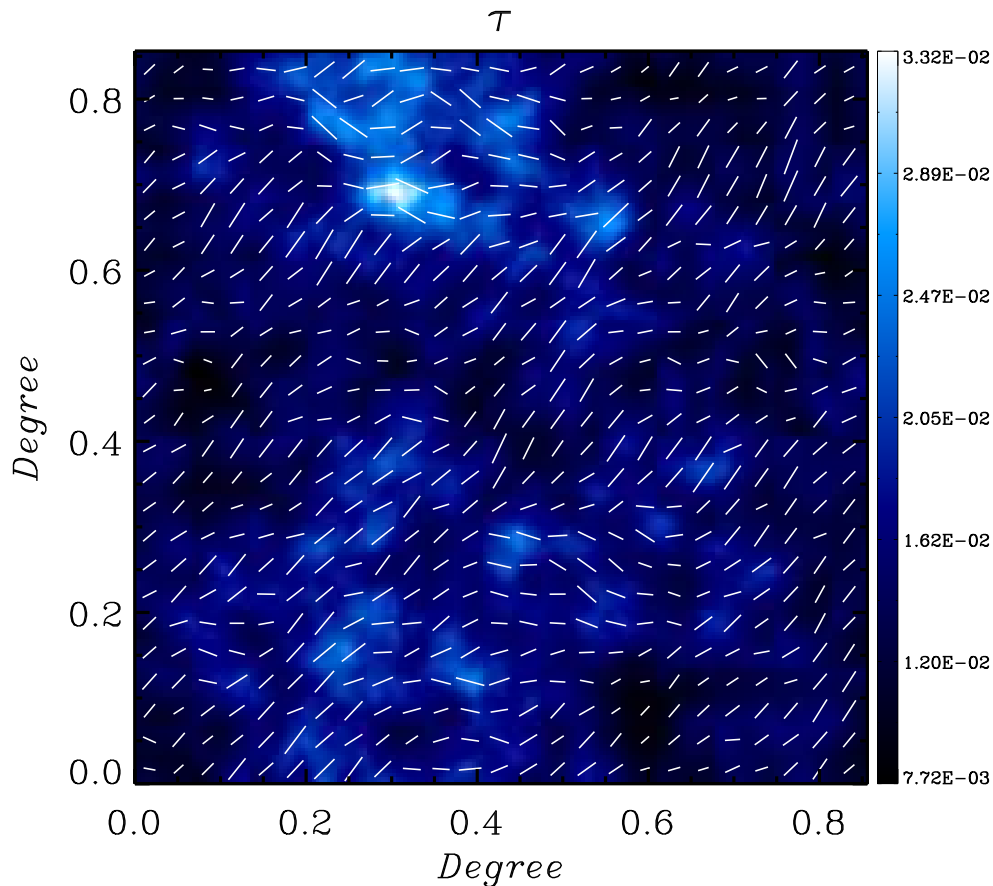


FIG. 2: Map of optical depth (color scale) and direction of polarization (shown by sticks denoting the orientation of the electric field) at each location in a typical map for the WMAP3 cosmology and the f250 ionization model. Note that the polarization amplitude is proportional to the optical depth (and also to the primordial quadrupole at that location), and that the amplitude of the polarization is *not* proportional to the length of the sticks.

Since similar results are obtained for a_{20} 's and a_{21} , we conclude that we can reasonably consider the a_{2m} 's to be constant within a box. For the sake of accuracy we will however allow them to vary between boxes but enforce the correct correlation properties. We do so by considering the $a_{2m}(z)$ as a multivariate Gaussian field with the previously computed correlation matrix given in Eq. 11.

Once we generated this set of $a_{2m}(z)$, it is straightforward applying Eq. 5 to propagate a photon plane through the boxes to generate a set of τ_T , Q and U maps. Note that care is taken during this stage to rotate and translate the boxes by random amounts to avoid any artifacts due to the fact that the boxes stems from a single initial condition realization. From these Q and U maps, we can easily measure the E and B mode power spectra in the flat sky approximation as well as generate a set of E and B mode maps (see for example Okamoto and Hu [29]).

IV. RESULTS

A typical result is shown in Figure 2. The optical depth fluctuations are substantial, with peak to peak variations larger than ± 0.01 . Note that these optical depth fluctuations are comparable to or larger than the Thomson optical depths along lines of sight through the centers of large galaxy clusters, the most massive collapsed objects in the local universe. This is easy to understand: the central regions of galaxy clusters today are overdense relative to the

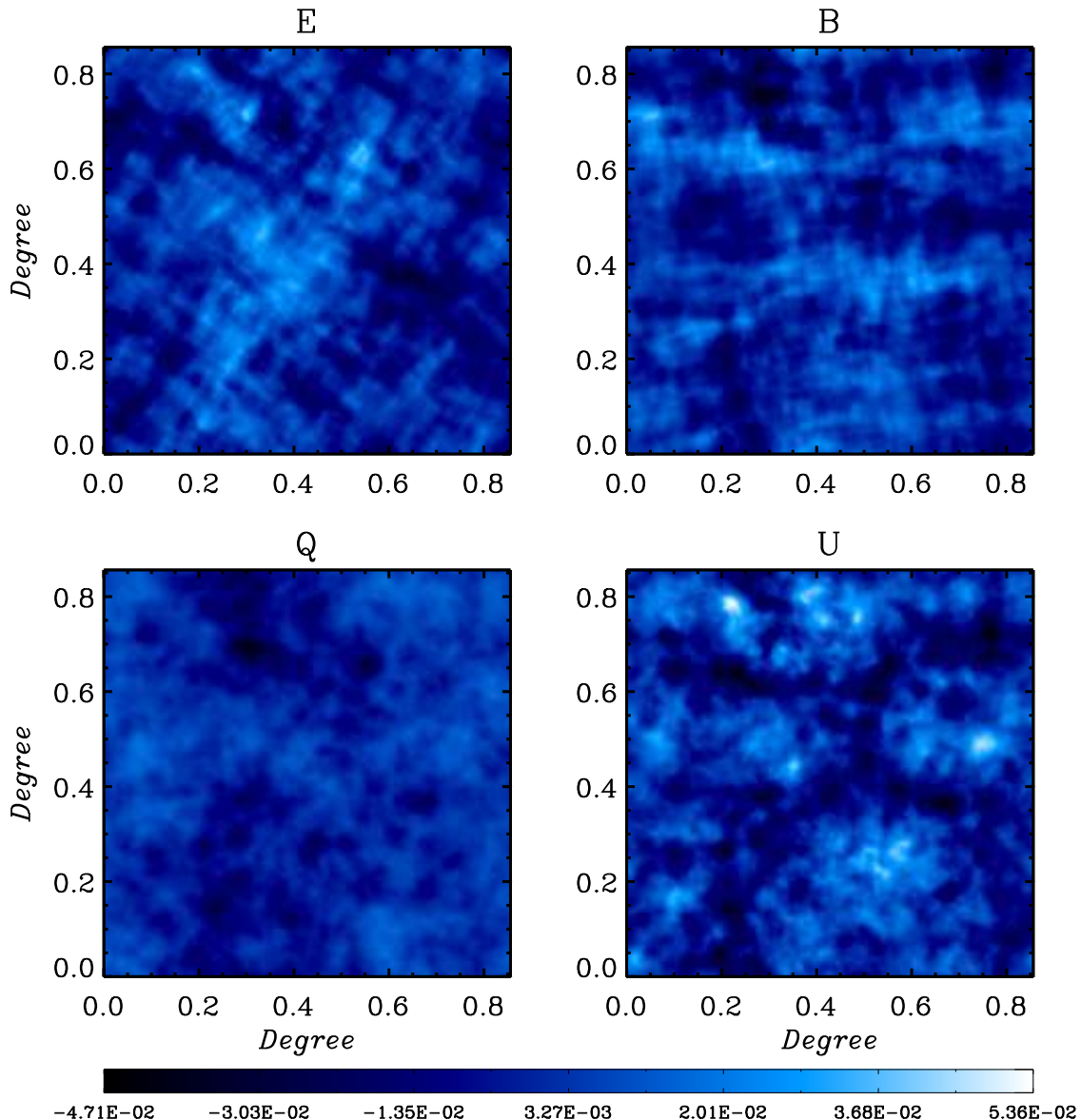


FIG. 3: Maps showing polarization maps for a typical realization for the WMAP3 cosmology and the f250 ionization model. Top panels show E and B maps, while bottom panels show Q and U maps. The mean was subtracted from each of this map to ease the comparison.

background density by factors of order 10^3 or 10^4 . The universe at redshift 9 was denser by a factor of 10^3 , so a path length on the order of 1 physical Mpc will have an optical depth comparable to a massive cluster in the local universe. The typical scale of the fluctuations is arcminutes. The direction of the polarization depends on the redshift that is contributing the scattering, since the quadrupole is highly coherent within a single simulation box length. Scattering events that are widely separated in redshift should have polarization angles that are largely uncorrelated. It is evident that the largest optical depth fluctuations correspond to scattering at comparable redshifts, although there is a noticeable dispersion in the polarization angles.

An important question is how this secondary scattering shows up as E-modes or B-modes. This is shown in Figure 3. There is a difference in the mean values of the two maps, since the first order scattering effect gives only EE correlations, but the fluctuations around the mean are of equal amplitudes in the EE and BB maps. By comparison the bottom panels show the Q and U maps, where it is evident that there is a large asymmetry, with much more power appearing in one (U in this case). This is easy to understand: if the scattering was a pure Gaussian isotropic

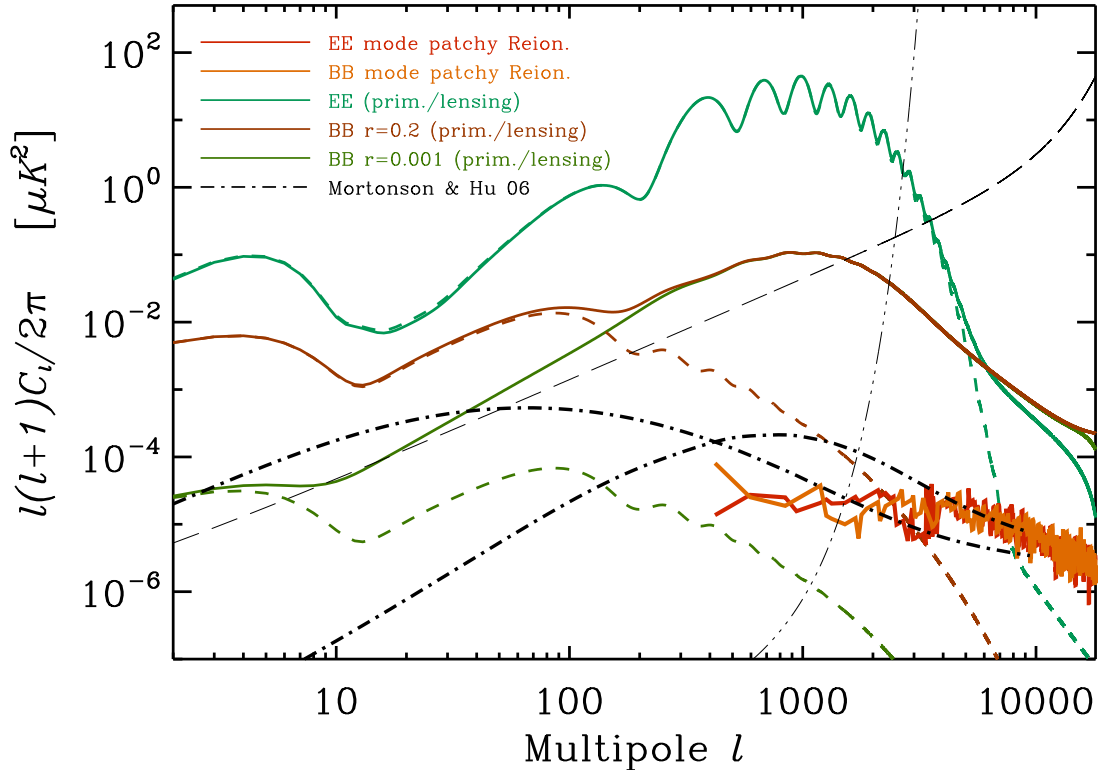


FIG. 4: Angular power spectrum of EE and BB polarization anisotropy, compared with primordial EE and BB signals (tensor to scalar ratio, $r=0.2$) and EE and BB signals including the effects of gravitational lensing (solid) or not (dashed). Several analytical computations as in Mortonson and Hu [5] are shown as well. The model that peaks around $\ell \simeq 80$ receives most of its contribution from $\simeq 200$ Mpc (comoving) bubbles whereas the one that peaks around $\ell \simeq 800$ is dominated by the contribution of $\simeq 40$ Mpc (comoving) bubbles. Note however that this model is not meant to reproduce our simulations (see text for details). The power level is smaller than the lensing-induced BB signal by several orders of magnitude on small scales. Planck sensitivity is shown by the dash-triple dot line, while an estimate for something like ACT or SPTPol is shown as a dashed line for a bin of width $\Delta\ell = 10$. For comparison, we also display an additional BB spectrum with $r=0.001$.

random field with a coherent quadrupole direction the result would be exactly equal power in EE and BB, but it would be possible to choose coordinates such that *all* of the power is in a single Stokes component Q or U (all of the signal with a single polarization angle). Working in EE and BB confuses the issue in this case. The coherence of the fluctuations in terms of Q and U suggest that it should indeed be possible (given sufficient signal to noise) to reconstruct the primordial quadrupole at specific locations during the epoch of reionization, given an estimate of the scattering optical depth.

The nature of E and B modes and the apparent excess in U over Q can be seen in the structure of the E and B maps. The E maps have clear structures oriented at 45 degrees, while the B maps have a tendency for structure in the horizontal and vertical directions. By construction, the E maps must have the structure varying along or orthogonal to the direction that the polarization is oriented, while the B maps will evolve at 45 degrees to the polarization direction. With most of the polarization being in Stokes U (i.e., at ± 45 degrees, this requires that the E modes will have structure mainly banded in the diagonal directions with the B modes showing banding along the axes. The polarization pattern from reionization is unlikely to show much resemblance to anything from the early universe.

Similarly, the separation in Q and U suggests that this may not be a serious impediment for cleaning of lensing. Lensing affects Q and U equally, so it should be always possible to find at least some modes that are useful for lensing reconstructions. Some careful investigations are currently underway to see whether this is indeed the case.

This signal might however provide a floor to any ability to measure either inflationary gravity wave-induced CMB polarization or do lensing reconstruction. This is shown in Figure 4. In this case it appears that these secondary

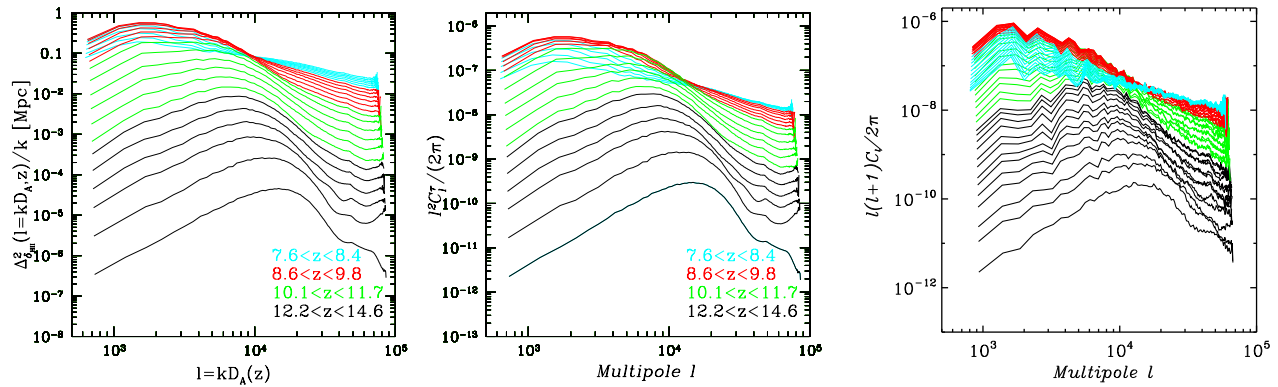


FIG. 5: Measured angular power spectra of individual simulation volumes at different redshifts, showing (left panel) the projection of the 3D power spectrum of the ionized hydrogen distribution using the Limber approximation, (middle) the angular power spectrum of the optical depth maps at each redshift deduced from this 3D power spectrum and (right) the measured angular power spectra for each redshift.

anisotropies will limit removal of lensing signals beyond the level of 1% in the power (10% in amplitude). The lensing reconstruction depends on the non-Gaussianity of the signal, so the power spectrum is not necessarily the best place to do this comparison. The maps are clearly non-Gaussian.

This is in rough agreement with Mortonson and Hu [5] and Liu et al. [4], and the level is comparable to that found in Baumann and Cooray [30]. However, the latter work looked at the contribution due to scattering in the fully ionized universe, and is a component that should be added to this signal. The coherence of the quadrupole in its direction is not expected for the superposition of scattering extending from the local universe out to distances corresponding to the epoch of reionization.

As carefully addressed in Mortonson and Hu [5] and Liu et al. [4], a crucial consideration for polarization anisotropy is the size of the characteristic ionized regions. The larger regions considered by the former paper are comparable to the simulation volume and thus it is difficult to explicitly compare results (see Fig. 4). Note that those results would certainly limit our ability to measure at low multipoles primordial B modes with a tensor to scalar ratio around 0.005. However, such large scale bubbles do not occur in our simulations. On the other hand, if the bubble distribution of Mortonson and Hu [5] is made to reproduce the one observed in our simulations –by typically adjusting the properties of the distribution of bubbles and its evolution– then the analytical computations can be in reasonable agreement with ours (see Fig. 4). We leave a more detailed comparison between this analytical model and our results for future work.

We find somewhat more small scale power, but the simulations don't have sufficient volume to accurately probe degree scale anisotropy. Our calculation is similar to that of Liu et al. [4], but with a more careful treatment of the process of reionization and an evolving quadrupole. Note that ignoring the evolution of the quadrupole will lead to nearly exactly equal EE and BB polarization, since the generated anisotropy will have the same plane of polarization and there is a coordinate system in which the signal is purely Stokes Q or Stokes U. A statistically isotropic amplitude distribution with a fixed polarization direction will necessarily have an equal number of modes parallel or perpendicular to the polarization direction as at ± 45 degrees.

V. DISCUSSION

The *rms* polarization signal on small scales due to the inhomogeneous process of the ionization of the universe at $z \sim 10$ is relatively small, on the order of $0.01 \mu K$, much smaller than the anisotropy induced by gravitational lensing of the primordial fluctuations. The signal has a unique signature, in that the polarization angle should be relatively constant over degree scales, with amplitude variations on scales of several arcminutes. This is a highly non-generic polarization anisotropy and is not what is expected from either gravitational lensing or primordial fluctuations. This is in line with previous expectations, although the non-Gaussianity of the optical depth distribution leads to some surprisingly large fluctuations at a few locations (approaching $0.1 \mu K$). This directional coherence should make the largest signals due to inhomogeneous ionization relatively easy to isolate, should experiments achieve the necessary very low noise levels. Note that this separation will also benefit from the mapping of E modes on large scales (B

modes signal is expected to be weaker there) where the reionization signature is averaged over the size of the horizon (Yadav and Wandelt [31]). The small scale patchy reionization would appear as an excess of power on smaller scales but with the same direction.

The signal will provide an ambitious target for upcoming CMB experiments. Noise curves for Planck [38] ($\sigma = 2.3 \mu\text{K}/5.0'$ fwhm, 0.85% of the sky) and rough estimates for ACT (Atacama Cosmology Telescope; Kosowsky [35]) and SPTPol (South Pole Telescope; Ruhl et al. [36]) ($\sigma = 2.0 \mu\text{K}/1.7'$ fwhm, 0.25% of the sky) are shown in Figure 4. The noise levels are orders of magnitude above what is required to image the polarization from inhomogeneous reionization. However, the non-Gaussianity of the signal means that it may be possible to detect some of this signal with near future instrumentation. Our computations also suggest that experiments targetting large scale measurements of the BB modes (*e.g.* SPIDER or EBEX) should not be concerned about this source of contamination. Note that our simulation size does not allow nor support the kind of very large bubbles considered by Mortonson and Hu [5] as displayed in Figure 4.

If we were to consider a dedicated survey, a very wide dish like the Large Millimeter Telescope 50m dish ($\Theta_{fwhm} = 0.07'$ at 100GHz) would be appropriate. Since our signal is about $\sigma = 0.01 \mu\text{K}$, and since current millimeter detectors achieve sensitivities of $200 \mu\text{K} \sqrt{s}$ at 100GHz, observing our signal with a signal to noise of 1 per beam would require observing for N_{days} days with N_{det} detectors with $N_{days} N_{det} \simeq 4600$. Note that focal planes being currently developed encompass several thousand detectors.

Alternatively, an independent and complementary approach proposed recently for deriving the optical depth fluctuations from patchy reionization is by using good quality redshifted 21-cm maps when such maps become available in the future (Holder et al. [32]).

Even with large non-Gaussianity, the Limber approximation (Kaiser [33], Limber [34]) is still sound. This is evident from Figure 5. The left panel essentially shows the result of calculating the 3D power spectrum of each box and using the Limber approximation to estimate the angular power spectrum while the right panel first projects the ionized distribution and then calculates the angular power spectrum directly. As long as the ionization distribution is relatively constant over the light crossing time of the typical fluctuations then one expects the Limber approximation to hold. We don't allow evolution within a single box as we make the maps, so it is possible that there is some additional signal coming from regions where the ionization structure is evolving rapidly. This may be of particular importance when regions are seeing several ionizing sources simultaneously.

As we discussed in detail in Section II, we simulate several reionization scenarios with varying photon production efficiency, f_γ , level of sub-cell gas clumping and background cosmology. The effect of these variations on the polarization signal is displayed in Fig.6. The results prove fairly robust and largely dependent of the background cosmology. However, some interesting dependence on the reionization scenarios is observed. In particular, the polarization signal is higher (by factor of $\sim 2 - 3$ in C_ℓ 's, for most of the range, but up to an order of magnitude at $\ell \sim 4000$) in extended-reionization scenarios (f250C cases) or high source efficiency (corresponding to large ionized bubble sizes) scenarios (f2000 and f2000C) compared to scenarios which lack both of these characteristics (f250 cases). Furthermore, the high source efficiency scenarios have somewhat more power at large scales, as expected. All these variations are relatively small, however, which combined with the weakness of the polarization signal makes it unlikely that polarization measurements would be used to distinguish different reionization scenarios.

The results presented in this work are based on reionization simulations which do not resolve the smallest atomically-cooling halos, with masses from $\sim 10^8$ to $\sim 2 \times 10^9 M_\odot$. Smaller-box, higher-resolution radiative transfer simulations which included these halos Iliev et al. [13] showed that the presence of low-mass sources results in self-regulation of the reionization process, whereby τ_{es} is boosted, while the large-scale structure of reionization and its end are not affected. The last feature is due to the strong suppression of these low-mass sources due to Jeans-mass filtering in the ionized regions. We expect that this self-regulation would not affect our current results significantly since the CMB polarization signal from the patchiness is dominated by the large bubbles. We should expect some boost in the power due to the higher optical depth and more extended nature of these reionization scenarios. The full calculation of this effect is still difficult, however, since the small computational box sizes currently required in order to resolve the low-mass sources would result in a large cosmic variance, in addition to underestimating the large-scale power of the ionization fluctuations.

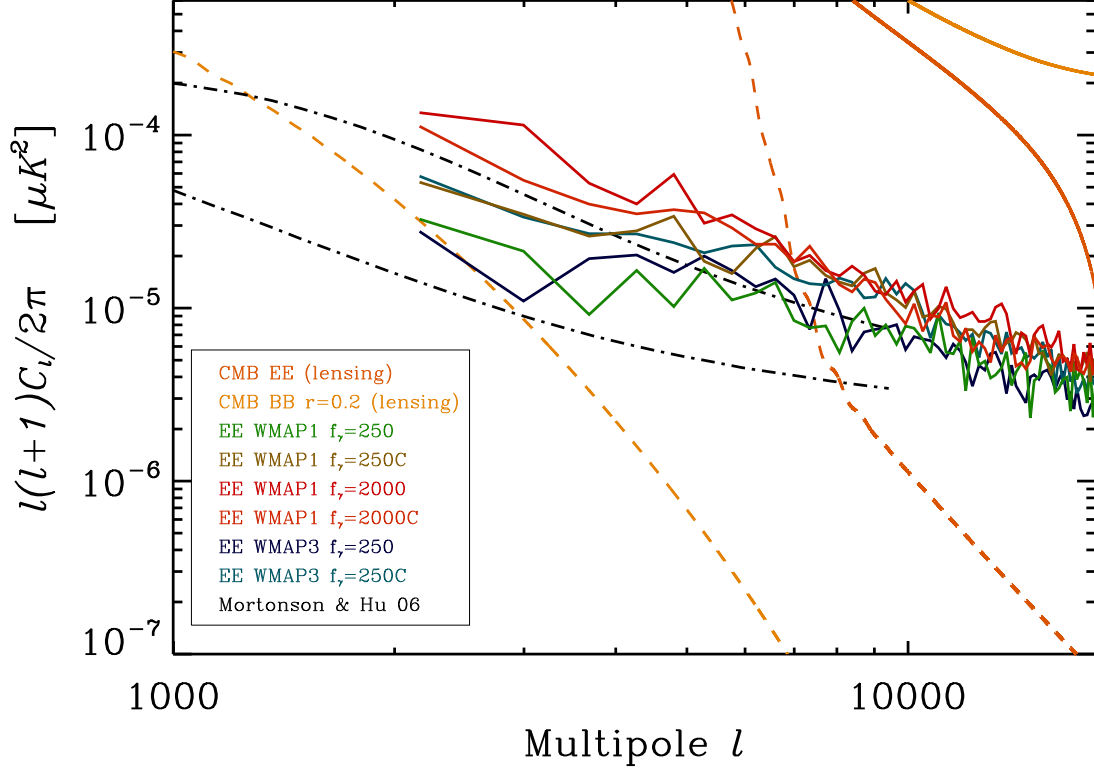


FIG. 6: Angular power spectra of EE polarization generated with various assumptions concerning either the cosmology (WMAP1 versus WMAP3 model) or the physics of reionization (various photon production efficiency, f_r , and with or without sub-cell gas clumping), as labelled by color. The primordial CMB is in solid line whereas the lensed one is in solid line. Analytics computation as in Fig. 4.

Acknowledgments

We thank Wayne Hu and Michael Mortonson for constructive exchanges.

-
- [1] L. Page, G. Hinshaw, E. Komatsu, M. R. Nolta, D. N. Spergel, C. L. Bennett, C. Barnes, R. Bean, O. Dore', M. Halpern, et al., ArXiv Astrophysics e-prints (2006), astro-ph/0603450.
 - [2] J. Weller, *Astrophys. J. Lett.* **527**, L1 (1999), astro-ph/9908033.
 - [3] W. Hu, *Astrophys. J.* **529**, 12 (2000), astro-ph/9907103.
 - [4] G.-C. Liu, N. Sugiyama, A. J. Benson, C. G. Lacey, and A. Nusser, *Astrophys. J.* **561**, 504 (2001), astro-ph/0101368.
 - [5] M. J. Mortonson and W. Hu, ArXiv Astrophysics e-prints (2006), astro-ph/0607652.
 - [6] G. Mellema, I. T. Iliev, U.-L. Pen, and P. R. Shapiro, *MNRAS* **372**, 679 (2006), astro-ph/0603518.
 - [7] I. T. Iliev, U.-L. Pen, J. Richard Bond, G. Mellema, and P. R. Shapiro, *New Astronomy Review* **50**, 909 (2006), astro-ph/0607209.
 - [8] I. T. Iliev, U.-L. Pen, J. R. Bond, G. Mellema, and P. R. Shapiro, submitted to *MNRAS* (2006), astro-ph/0609592.
 - [9] L. Knox and Y.-S. Song, *Physical Review Letters* **89**, 011303 (2002), astro-ph/0202286.
 - [10] U. Seljak and C. M. Hirata, *Phys. Rev. D* **69**, 043005 (2004), astro-ph/0310163.
 - [11] I. T. Iliev, G. Mellema, U.-L. Pen, H. Merz, P. R. Shapiro, and M. A. Alvarez, *MNRAS* **369**, 1625 (2006), astro-ph/0512187.
 - [12] G. Mellema, I. T. Iliev, U.-L. Pen, and P. R. Shapiro, *MNRAS* **372**, 679 (2006), astro-ph/0603518.
 - [13] I. T. Iliev, G. Mellema, P. R. Shapiro, and U.-L. Pen, *MNRAS* in press (2006), astro-ph/0607517.
 - [14] H. Merz, U.-L. Pen, and H. Trac, *New Astronomy* **10**, 393 (2005).

- [15] D. N. Spergel *et al.*, *Astrophys. J. Suppl.* **148**, 175 (2003).
- [16] D. N. Spergel *et al.*, ArXiv Astrophysics e-prints (arXiv:astro-ph/0603449) (2006), arXiv:astro-ph/0603449.
- [17] U. Seljak and M. Zaldarriaga, *Astrophys. J.* **469**, 437 (1996).
- [18] G. Mellema, I. T. Iliev, M. A. Alvarez, and P. R. Shapiro, *New Astronomy* **11**, 374 (2006).
- [19] I. T. Iliev, B. Ciardi, M. A. Alvarez, A. Maselli, A. Ferrara, N. Y. Gnedin, G. Mellema, T. Nakamoto, M. L. Norman, A. O. Razoumov, et al., *MNRAS* **371**, 1057 (2006), astro-ph/0603199.
- [20] P. R. Shapiro, I. T. Iliev, and A. C. Raga, *MNRAS* **348**, 753 (2004).
- [21] I. T. Iliev, P. R. Shapiro, and A. C. Raga, *MNRAS* **361**, 405 (2005).
- [22] I. T. Iliev, E. Scannapieco, and P. R. Shapiro, *Astrophys. J.* **624**, 491 (2005).
- [23] B. Ciardi, E. Scannapieco, F. Stoehr, A. Ferrara, I. T. Iliev, and P. R. Shapiro, *MNRAS* **366**, 689 (2006).
- [24] M. McQuinn, A. Lidz, O. Zahn, S. Dutta, L. Hernquist, and M. Zaldarriaga, ArXiv Astrophysics e-prints (2006), astro-ph/0610094.
- [25] M. Zaldarriaga and U. Seljak, *Phys. Rev. D* **55**, 1830 (1997), astro-ph/9609170.
- [26] A. Amblard and M. White, *New Astronomy* **10**, 417 (2005), astro-ph/0409063.
- [27] J. Portsmouth, *Phys. Rev. D* **70**, 063504 (2004), astro-ph/0402173.
- [28] W. Hu and M. White, *Phys. Rev. D* **56**, 596 (1997), astro-ph/9702170.
- [29] T. Okamoto and W. Hu, *Phys. Rev. D* **66**, 063008 (2002), astro-ph/0206155.
- [30] D. Baumann and A. Cooray, *New Astronomy Review* **47**, 839 (2003), astro-ph/0304416.
- [31] A. P. Yadav and B. D. Wandelt, *Phys. Rev. D* **71**, 123004 (2005), astro-ph/0505386.
- [32] G. Holder, I. T. Iliev, and G. Mellema, ArXiv Astrophysics e-prints (2006), astro-ph/0609689.
- [33] N. Kaiser, *Astrophys. J.* **388**, 272 (1992).
- [34] D. N. Limber, *Astrophys. J.* **117**, 134 (1953).
- [35] A. Kosowsky, *New Astronomy Review* **50**, 969 (2006), astro-ph/0608549.
- [36] J. Ruhl, P. A. R. Ade, J. E. Carlstrom, H.-M. Cho, T. Crawford, M. Dobbs, C. H. Greer, N. w. Halverson, W. L. Holzapfel, T. M. Lanting, et al., in *Z-Spec: a broadband millimeter-wave grating spectrometer: design, construction, and first cryogenic measurements*. Edited by Bradford, C. Matt; Ade, Peter A. R.; Aguirre, James E.; Bock, James J.; Dragovan, Mark; Duband, Lionel; Earle, Lieko; Glenn, Jason; Matsuhara, Hideo; Naylor, Bret J.; Nguyen, Hien T.; Yun, Minhee; Zmuidzinas, Jonas. *Proceedings of the SPIE, Volume 5498*, pp. 11-29 (2004)., edited by C. M. Bradford, P. A. R. Ade, J. E. Aguirre, J. J. Bock, M. Dragovan, L. Duband, L. Earle, J. Glenn, H. Matsuhara, B. J. Naylor, et al. (2004), pp. 11–29.
- [37] $3248 = N_{nodes} \times (512 - 2 \times 24)$, where $N_{nodes} = 7$ (with 4 processors each), 512 cells is the Fourier transform size and 24 cells is the buffer zone needed for correct force matching on each side of the cube.
- [38] <http://www.rssd.esa.int/Planck>